Trends in and closure of the Atmospheric Angular Momentum balance in the 20th century in ERA-20C

Menno Veerman

February 15, 2018

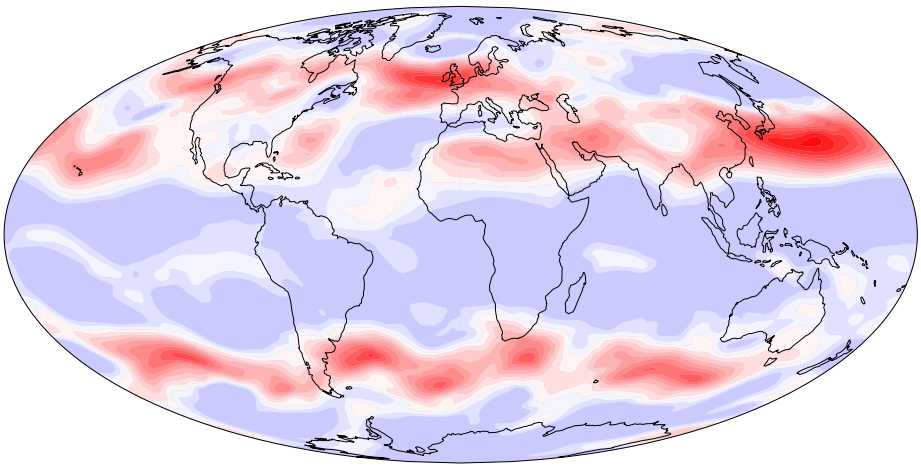

MSc Thesis

Meteorology and Air Quality
Wageningen University

Title:	Trends in and closure of the Atmospheric Angular Momentum balance in the 20th century in ERA-20C
Date:	15-02-2017
Author:	Menno Veerman
Reg. No.:	931206860090
Supervisor:	Chiel van Heerwaarden
Examiners	Chiel van Heerwaarden Bert Holtslag

Abstract

It is well known that global warming in the 20th century has influenced the global circulation of the atmophere. The angular momentum of the atmosphere (AAM), a measure of its the rotation around the axis of the earth, is a useful quantity to investigate changes in the global atmospheric circulation. In this study, 20th century trends in the AAM budget have been determined using the ERA-20c reanalysis data of the European Center of Medium-Range Weather Forecasts (ECMWF). In addition, the closure of the AAM balance has been determined to assess the ability of ERA-20c to conserve angular momentum.

The total AAM has increased slightly in the 20th century, which has been associated mainly with two changes in the relative (zonal wind) AAM component. The relative AAM has increased in both the lower stratosphere and the tropical upper-troposphere, and has mainly been redistributed to higher latitudes in the mid-latitudes. As several studies have pointed out as well, these trends can be related to the warming trend in the troposphere and the cooling in the lower stratosphere also observed in this study, both as a result of the increase in the atmospheric CO_2 concentration. The omega-AAM, which represents the rotation of the atmosherd along with the earth, shows no clear trend, but a spurious peak around 1920. This peak is associated with a global increase in surface pressure and is interpreted as an artifact of changes in the amount of assimilated observations.

It is also found that the AAM balance it not well closed in ERA-20c, which is mainly the result of the assimilation observations during the production of the reanalysis. In addition, the temporal evolutions of the balance residuals and amount of zonal wind observations show several similarities in the early half of the 20th century. The trends in the AAM budget found in ERA-20c are therefore likely also affected by changes in the number of assimilated observations and should be carefully validated with other reanalyses in further research.

Contents

1 Introduction

Numerous studies have shown that global warming (IPCC, 2013) can cause changes in the global atmospheric circulation: In reanalysis data of the late 20th century, Hu and Fu (2007) found a poleward shift of the boundaries of the Hadley circulation. Climate models also predict a further widening of the Hadley cells in the 21st century due to global warming (Lu et al., 2007). A late 20th century poleward shift and intensification of the storm tracks has been observed by Chen and Held (2007). These trends have been attributed to both the decreasing stratospheric ozone concentrations and the increasing CO_2-concentrations in the 20th century (Chen and Held, 2007; Lorenz and DeWeaver, 2007). These changes in the atmospheric circulation are associated with changes in the global distribution of zonal winds.

A useful concept to study the global atmospheric circulation is angular momentum. The atmospheric angular momentum (AAM) is a quantity related to both the global surface pressure and the global zonal wind distribution (see Sect. 2.1). It is a measure of the rotation of the whole atmosphere around the north-south axis of the earth. Angular momentum is exchanged between the atmosphere and earth by torques, which is the angular form of a force (see Sect. 2.2). The two main torques acting on the atmosphere are the result of the friction at the surface of the earth and gradients in atmospheric pressure across orographic features (Peixoto and Oort, 1992).

Although angular momentum is a conserved quantity, it is often not conserved in weather and climate models: a large AAM imbalance in reanalysis data was found by Huang et al. (1999), which they attributed to the parameterizations of the gravity wave drag. Comparable AAM imbalances in other data sets have been reported by e.g. Berrisford et al. (2011) and Madden and Speth (1995). Berrisford et al. (2011) also observed that in two reanalysis data sets of the European Center of Medium-Range Weather Forecasts (ECMWF), ERA-40 and ERA-Interim, the closure of the AAM balance has improved in time. They also found a better closure in the more recent ERA-Interim, indicating the higher quality of this data set (Berrisford et al., 2011). The degree to which AAM is actually conserved in weather or climate models can thus be used to assess model performance and the accuracy of the data (e.g. Huang et al., 1999; Berrisford et al., 2011).

Long-term changes in AAM have been related to trends or variations in the atmospheric circulation by several studies (e.g. Huang et al., 2001; Räisänen, 2003; Huang et al., 2003). Studies have also shown a good correlation between AAM and the length of a day (e.g. Rosen and Salstein, 1983): AAM fluctuations are accompanied by opposite fluctuations in the angular momentum of the earth, and thus its rotation speed. An increase in AAM due to an increasing atmospheric CO_2-concentration in climate models has been shown by e.g. Huang et al. (2001), Räisänen (2003) and Paek and Huang (2013). This response to CO_2 has been attributed mainly to an increase in stratospheric and upper-tropospheric zonal winds, which results in a stronger meridional temperature gradients around the tropopause (e.g. Huang et al., 2001; Räisänen, 2003).

Inter-annual AAM variations have been related to atmospheric variabilities such as the El-Niño Southern Oscillation or the Quasi-Biennial Oscillation (Chao, 1989; Abarca del Rio et al., 2000; Rosen et al., 1984; Huang et al., 2003). These oscillations correspond to fluctuations in zonal wind speed, and thus AAM, in the tropical troposphere and stratosphere, respectively (Holton and Hakim, 2012). On shorter time-scales, AAM also has a clear variability (e.g. Rosen and Salstein, 1983; Weickmann et al., 1997; Anderson and Rosen, 1983), such as an annual cycle related to the seasonal shifts in the jet stream (Rosen and Salstein, 1983).

Most previous studies on AAM changes in the 20th century studied its temporal variability on seasonal to decadal time scales (e.g. Rosen and Salstein, 1983; Chao, 1989; Huang et al., 2003; Paek and Huang, 2012, 2013) or investigated trends in only the second half of the 20th century (del Rio, 1999). The

latter is likely associated with the lack of sufficient upper-air and satellite observations in the early 20th century (Hersbach et al., 2015). However, due to natural climate variabilities on decadal scales, using only half a century might be insufficient to accurately determine long-term AAM trends (Huang et al., 2003). Analysing the 20CR reanalysis (Compo et al., 2011), produced by the National Center for Environmental Prediction/National Center for Atmospheric Research (NCEP/NCAR), Paek and Huang (2012) already observed an increase in relative AAM since 1871. This has been attributed mainly to an increase in zonal wind speeds in the upper troposphere (Paek and Huang, 2012). However, they also found that the evolution of AAM in the 20CR data in the second half of the 20th century did not match the evolution found in other reanalysis data sets (Paek and Huang, 2012), indicating that the reliability of the AAM trend in 20CR may be doubted (Paek and Huang, 2012).

In this study, the first goal is to determine and analyse trends in the AAM budget during the 20th century using the ERA-20c reanalysis data set, which was produced in 2014 by the ECMWF (Poli et al., 2016). For this trend analysis, changes in both the global integrals and the meridional distributions of the monthly mean AAM and the torques are studied. In addition, changes in the zonal wind and temperature distributions are determined. Understanding how trends in the AAM budget relate to trends in the zonal wind and temperature, caused by for example the increasing CO_2 and decreasing stratospheric ozone concentrations (IPCC, 2013), can aid to improve our knowledge on the effects of e.g. global warming on the atmosphere. The second goal of this study is to determine the closure of the AAM balance, which shows how well angular momentum is actually conserved in the ERA-20c reanalysis. The AAM balance closure is an indication of model performance (Berrisford et al., 2011) and also serves to assess the reliability of the trends in the AAM budget. The two main research questions on which this study is based are therefore:

1. How well is the atmospheric angular momentum balance closed in the ECMWF ERA-20c reanalysis and how has this closure changed during the 20th century?

2. What have been the trends in the atmospheric angular momentum budget during the 20th century and how are these trends related to the 20th century climate change?

A more elaborate background on the concept of angular momentum, the torques, and their relation to the atmospheric circulation is provided in Section 2. In Section 3, the data and the methods used in this study are given. The results are given in Section 4; first the results concerning the closure of the AAM balance (Sect. 4.1) and subsequently the trend analysis (Sect. 4.2). A more elaborate discussion of the results is provided in Section 5 and the conclusions are given in Section 6.

2 Theoretical background

In this section, the theoretical background of this study is given. First, the concept of angular momentum is introduced, its connection to the atmospheric, and how this quantity is related to the global atmospheric circulation. Subsequently, an explanation is given of torques, which cause the exchange of angular momentum between the earth and the atmosphere.

2.1 Angular momentum

Angular momentum is a quantity related to the rotation of an object, analogously to linear momentum being a measure of movement in a straigth line. The angular momentum of the solid earth, the oceans and the atmosphere combined is caused by the rotation of the earth about its axis with an approximately constant angular velocity Ω ($\approx 7.29 \cdot 10^{-5}$ s^{-1}) (Peixoto and Oort, 1992). Similar to linear momentum, angular momentum is a conserved quantity. Assuming external forces such as tides are negligible, the total angular momentum of the earth system therefore remains constant (Peixoto and Oort, 1992). However, angular momentum is exchanged between the earth, the oceans, and the atmosphere. The atmospheric angular momentum (AAM) is therefore not necessarily constant, but its tendency should equal its exchange with the earth and oceans.

The total or absolute AAM can be divided into an omega (Ω) component, also known as the 'Earth'-component (e.g. Weickmann et al., 1997), and a relative component. The relative angular momentum per unit volume of an air parcel (m_r) is due to its zonal (west-east) movement relative the earth. m_r is thus related to the zonal component (u) of the horizontal wind vector:

$$m_r = \rho \, u \, a \cos\phi, \tag{1}$$

where ρ is the density of the air parcel, a is the radius of the earth ($\approx 6,367,470$m) and ϕ is latitude. The $a\cos\phi$-term indicates that the distance to earth's rotation axis decreases with increasing latitude (Fig. 1). In Eq. 1, it is assumed that the height above the earth's surface is negligble compared to the radius of the earth.

The Ω-component of the angular momentum of an air parcel (m_Ω) is due to its rotation along with the earth with velocity $\Omega a \cos\phi$ (Fig. 1):

$$m_\Omega = \rho \, \Omega (a\cos\phi)^2. \tag{2}$$

The total angular momentum of an air parcel, which is the sum of both components, thus becomes:

$$m = \rho \, (u + \Omega \, a \cos\phi) a \cos\phi. \tag{3}$$

As Eq. 1 shows, the relative component of the angular momentum of the whole atmosphere is related to the meridional zonal wind distribution. For example, the predominant westerly (positive) zonal winds in the mid-latitudes (Fig. 2) are associated with a positive relative angular momentum (Fig. 3A), whereas the easterly (negative) zonal winds near the equator are associated with a negative relative angular momentum. Since earth's rotation (Ω) is almost constant, the Ω component depends mainly on the atmospheric mass distribution and on latitude (Eq. 2). As shown in Figure 3B, the Ω-component rapidly decreases towards the poles. It is also lower in mountainous regions (e.g. Rocky mountains, Himalaya, Andes) than in other areas at the same latitude (Fig. 3B), which is due to the decrease in pressure and thus atmospheric mass with height.

The magnitude of the Ω-component is much larger than that of the relative component (figs. 3A,B). Integrated over the whole atmosphere, the Ω-component of the AAM is on the order of $1.0 \cdot 10^{28}$ kg m^2 s^{-1},

whereas the relative component is only about $1.5 \cdot 10^{26}$ kg m^2 s^{-1} (e.g. Berrisford et al., 2011; Madden and Speth, 1995). Nevertheless, seasonal and annual fluctuations in the relative AAM component are usually larger than fluctuations in the Ω-component (Madden and Speth, 1995), due to e.g. the seasonal cycle or El-Niño's.

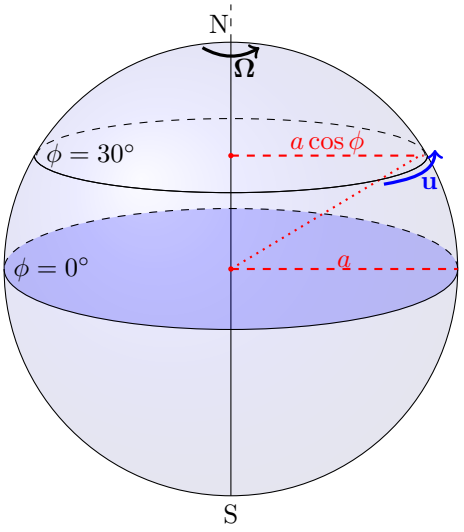

Figure 1: Sketch of the direction of rotation and the dependence of the radius on latitude. Adapted from Peixoto and Oort (1992).

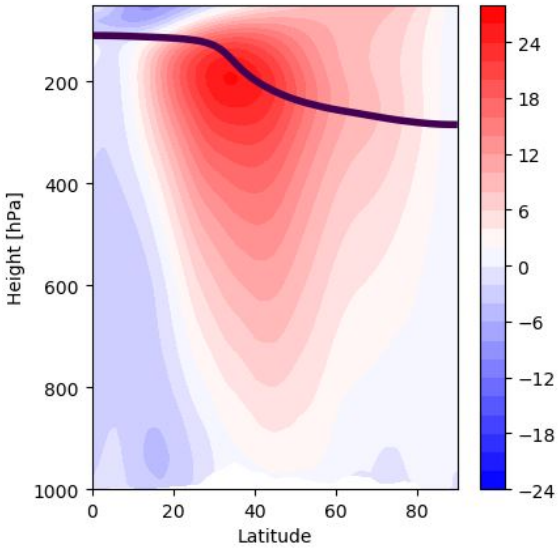

Figure 2: Latitude-height distribution of the mean zonal wind (m/s) in the northern hemisphere. The thick black line is the mean tropopause height.

The conservation of angular momentum is an important factor in the global atmospheric circulation (Schneider, 2006). In the tropical upper-troposphere, the mean meridional winds transport angular momentum poleward. Since the radius of the earth ($a\cos\phi$) decreases with latitude, conservation of angular momentum implies that the zonal wind (u) must increase (see Eq. 3). This results in the increasing westerly winds with increasing latitude near the subtropical upper-troposphere (Fig. 2), although the mean poleward wind does not conserve its angular momentum entirely (Schneider, 2006). Near the surface in the subtropics and mid-latitudes, the westerly wind speeds and thus the relative angular momentum are considerably lower (Fig. 2), because of the torques acting on the atmosphere (Sect. 2.2). Due to this loss of angular momentum to the earth, the relative angular momentum in the lower-troposphere becomes negative during the equatorward flow since the radius increases towards lower latitudes. This negative relative angular momentum corresponds to the easterly winds in the tropics (Fig. 2)

This circulation, which is known as the Hadley circulation, extents from the equator to about 30° latitude (Schneider, 2006). Around this latitude the meridional temperature gradient increases, which is indicated by the steepening tropopause slope in Figure 2. The larger temperature gradient is related to the strong increase in zonal wind speed with height, also known as the thermal wind balance (e.g. Holton and Hakim, 2012), causing the atmosphere to become baroclinically unstable (Schneider, 2006). This instability results in large eddies, which provide the further poleward transport of angular momentum to and within the mid-latitudes. This eddy transport of angular momentum results in the predominant westerly circulation in the mid-latitudes (Fig. 2; Schneider (2006)). Due to these westerly winds, angular momentum is transported from the atmosphere to the earth in the mid-latitudes, whereas the easterlies in lower latitudes result in an angular momentum transport to the atmosphere.

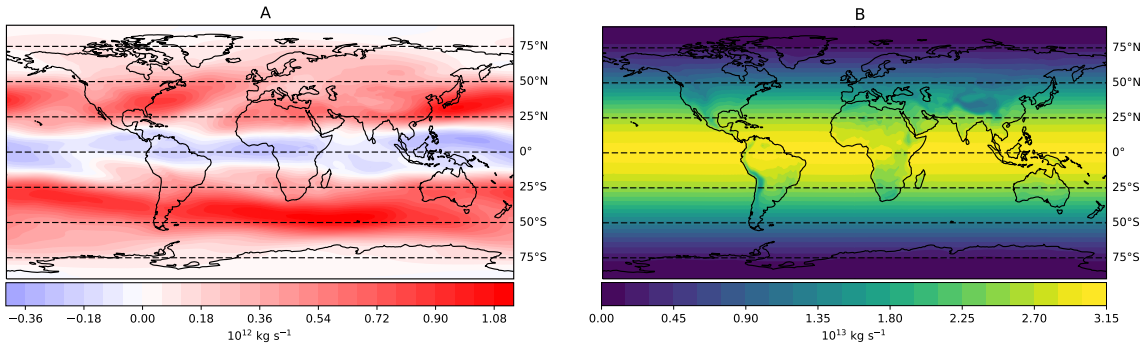

Figure 3: Spatial distribution of the vertical integrals of the relative (a) and Ω (b) angular monentum, averaged over the period 1900-2010. For more details about the calculations, see Section 3.2

2.2 Torques

The exchange of angular momentum between the earth and atmosphere is due to torques, the rotational form of a force. Whereas a force affects the velocity of an object by accelerating it, a torque change its rate of rotation or angular velocity. The torques (T) acting on the atmosphere are calculated as the product of the (drag) forces (τ) at the surface of the earth and the radius of the earth:

$$T = \tau a \cos \phi. \tag{4}$$

The two main torques that act between the atmosphere and the earth are the friction torque and the mountain torque (Peixoto and Oort, 1992). The friction torque is due to the turbulent drag associated with skin friction and depends on wind speed and the roughness of the surface. The mountain torque is related to pressure drag and is caused by surface pressure differences across orography. For example, if the pressure on one side of an mountain is higher than on the other side, the atmosphere exerts a torque in the direction of this pressure gradient. An negative eastward pressure gradient therefore results in an eastward mountain torque, thus a transport of angular momentum from the atmosphere to the earth.

There are several atmospheric processes associated with this mountain torque (Beljaars et al., 2004). In sufficiently stable conditions, part of the atmospheric flow is blocked by the orography, decelerating the flow and forcing it to go around the orography (Lott and Miller, 1997). The flow that is forced over a mountain induces gravity waves, which can propagate upward and thus transport angular momentum between the surface and higher atmospheric layers (Lott and Miller, 1997). Orographic features can also cause extra turbulence, which is known as the turbulent form drag (Beljaars et al., 2004). In climate models only large-scale orography is resolved due to their relatively coarse resolution. However, orography on scales smaller than the model resolution, also known as the sub-grid orography (ECMWF, 2013), also exerts a drag force on the atmosphere and therefore also contributes to the total torque (Beljaars et al., 2004). In climate models, this additional drag due to subgrid scale orography is therefore parameterized (Beljaars et al., 2004).

3 Methodology

The main goal of this research is to determine trends in the 20th century atmospheric angular momentum (AAM) budget and the closure of the AAM balance. In this section, first an overview is given of the data set used in the study. Subsequently, the AAM budget equations are explained, as well as the methods used to calculate the AAM budget. Last, a short description is given of additional methods used to study the closure of the AAM balance.

3.1 Data description

The data set used in this research is the ECMWF reanalysis of the twentieth century (ERA-20c), which was released in 2014 and covers the time period 1900-2010 (Poli et al., 2016). During the production of ERA-20c, only observations of surface pressure and marine surface wind have been assimilated (Poli et al., 2016). The data are retrieved on a regular latitude-longitude grid of 161 by 320 grid points, which gives a horizontal resolution of 1.125°x1.125° ($\approx$ 125x125 km near the equator). In the vertical, the data are retreived on all original 91 model levels, which prevents errors arising due to the vertical interpolation of variables to pressure levels (Trenberth, 1991). These 91 model levels form a hybrid coordinate system (Simmons and Burridge, 1981), which is terrain-following in the lower atmosphere and transitions to pressure levels in the upper atmosphere. The lowest model level equals the surface pressure, the highest model level is at 0.01 hPa.

The available temporal resolution of the data is three hours. For the trend analysis, however, the monthly means of the data are used to reduce data size and computation time. Since the focus of this research is on long-term trends, using monthly means should not affect the results. For the trend analysis, the entire time span of the data is used; the whole 20th century as well as the years 2000 up to 2010. In further reference, the full 111 year period is still referred to as the 20th century. The main variables of interest are the surface pressure, zonal wind and the parameterized gravity wave and turbulent surface stresses.

Both the forecast data and the analysis data of ERA-20c are available. The forecast data consists of all the 27-hour model forecasts, integrated each day from 6 UTC to 9 UTC the next day (Poli et al., 2013). The analysis data are the results of the assimilation of observations to each model forecast (Poli et al., 2013) and are therefore assumed to be more accurate. Observations have been assimilated after each 27-forecast, and the resulting analysis data were used as initial conditions for the next forecast (Poli et al., 2013). To study trends in the AAM budget, only the analysis data set is used. The closure of the AAM balance is investigated using both the forecast and the analysis data set.

3.2 AAM budget

To study 20th century trends in the AAM budget, the monthly mean total AAM, its relative and Ω components, and the monthly mean torques are calculated throughout the 20th century. Since the focus of this study is on trends in the angular momentum budget of the whole atmosphere, the terms of the AAM budget are integrated globally, i.e. over all latitudes, longitudes and model levels. However, the latitudinal contributions to the global trends are also determined, by only integrating the AAM budget terms in zonal direction. Investigating the zonal contributions to the trends is used to detect meridional shifts in the atmospheric circulation.

The total angular momentum of a column of air (M) can be obtained by integrating Eq. 3 vertically. This integral is approximated by a summation over all 91 model levels (Simmons and Burridge, 1981):

$$M = \frac{1}{g} \sum_{\eta=1}^{91} (u + \Omega\ a\cos\phi) a\cos\phi\ \Delta p_\eta, \tag{5}$$

where g and η are the gravitational acceleration (9.81 m s^{-2}) and the model level, respectively. Δp_η is the thickness (in Pa) of the atmospheric layer represented by each model level. By vertically integrating Eq. 1 and Eq. 2, the relative (M_r) and Ω (M_Ω) components of M are obtained as

$$M_r = \frac{1}{g} \sum_{\eta=1}^{91} u \; a \cos\phi \; \Delta p_\eta \tag{6}$$

and

$$M_\Omega = \frac{1}{g} \sum_{\eta=1}^{91} \Omega a^2 \cos^2\phi \; \Delta p_\eta = \frac{p_s}{g} \Omega a^2 \cos^2\phi, \tag{7}$$

respectively, where p_s is the surface pressure. As Eq. 6 shows, trends in M_r are mainly related to changes in the magnitude or meridional distribution of zonal winds (u). As shown by Eq. 7, M_Ω is due to the rotation of the mass of the atmosphere (p_s/g) around earth's axis along with the rotaton of the earth (Ω).

The global AAM is then obtained by integrating M (Eq. 5) over the surface of the earth, i.e. by summing over all 161 latitudes and 320 longitudes on the horizontal grid of the data:

$$AAM = a^2 \sum_{i=1}^{161} \sum_{j=1}^{320} M_{ij} \cos\phi_i \, \Delta\lambda_j \, \Delta\phi_i, \tag{8}$$

where $\Delta\lambda_j$ and $\Delta\phi_i$ are the grid spacings in longitudinal and latitudinal direction, respectively. The relative and Ω AAM components can be then obtained by integrating M_r (Eq. 6) and M_Ω (Eq. 7) globally, analogously to Eq. 8

As angular momentum is conserved, the rate of change of AAM should equal the sum of all torques. The global AAM balance can be derived as (see e.g. Holton and Hakim, 2012; Peixoto and Oort, 1992, for a more detailed derivation):

$$\frac{\mathrm{d}\; AAM}{\mathrm{d}\; t} = -\frac{1}{g}\left[p_s \frac{\partial \Phi_s}{\partial \lambda}\right] - \left[\tau_{gw} \; a \cos\phi\right] - \left[\tau_{ts} \; a \cos\phi\right], \tag{9}$$

where Φ_s, τ_{gw} and τ_{ts} are the surface geopotential height, the gravity wave stress and the turbulent surface stress, respectively. The square brackets on the right hand side of Eq. 9 denote global surface integrals (see Eq. 8). The first term of Eq. 9 is the monthly AAM tendency, which is the change in AAM between the first time steps (at 9 UTC) of consecutive months. The first term on the right hand side of Eq. 9 is the resolved mountain torque, which is calculated as the product of the surface pressure and the zonal gradient of the surface geopotential height. Because the data is periodic in zonal direction, the zonal gradient is calculated with spectral differentation (Johnson, 2011) using a fourier series of the geopotential height along a latitude circle. The second and third terms of Eq. 9 are the parameterized gravity wave torque and the parameterized frictional torque, respectively. It should be noted that there are no horizontal divergence terms in Eq. 9, because these should vanish upon the global integrations.

Although the focus of this study is on trends in AAM (Eq. 8) and the terms in the AAM budget (Eq. 9), trends in e.g. the zonal wind, air temperature and surface pressure are also determined. This helps the interpretation of the AAM trends and their relation with changes in climate and the atmospheric circulation.

3.3 Balance closure

Since angular momentum is a conserved quantity, the closure of the AAM balance is a measure of model performance (e.g. Berrisford et al., 2011; Huang et al., 1999). Due to the assimilaton of observations in the reanalysis, it may be expected that the AAM balance (Eq. 9) is not exactly closed (e.g.

Berrisford et al., 2011). Therefore, the balance residuals and the temporal evolution of the balance residuals are also studied. The residual of the AAM balance is calculated as the difference between the left and the right hand side of Eq. 9, that is, the AAM tendency minus the torques.

Both the analysis and forecast data (Sect. 3.1) are used to study the closure of the AAM balance. The balance in the analysis data is interesting, because this data set is used for the analysis of AAM trends in the 20th century. The balance in the forecast data is calculated to determine the closure of the AAM balance without the influence of the assimilation of observations. For this purpose, the full 3-hourly temporal resolution of the forecast data is used and the AAM tendencies are not calculated between consecutive forecasts. However, since each forecast represents a period of 27 hours, there is overlap between consecutive forecasts at 9 UTC (Poli et al., 2013). To calculate the tendency between 6 and 9 UTC in each forecast, 9 UTC is the last time step of the forecast, whereas it is the first time step of the next forecast to determine the tendency between 9 and 12 UTC. Because the balance closure in the forecast data does not depend on the assimilation of observations, it is assumed to be constant in time. Therefore, the AAM balance in the forecasts is only determined for the time periods 1900-1915 and 1995-2010 to limit the amount of data to be retrieved and computational time.

The observations that have been assimilated in the production of ERA-20c are also available in the data set (Hersbach et al., 2015) and are retrieved as well. Changes in the number of observations can affect the trend analysis (Poli et al., 2013) and the temporal evolution of the balance residuals in the analysis data (Berrisford et al., 2011). Therefore, the monthly amounts of assimilated zonal wind and surface pressure observations are also determined.

4 Results

In this section, the results of this study are presented and interpreted. First the results concerning the closure of the AAM balance are given (Sect. 4.1). This part focuses on the degree to which angular momentum is conserved in the ERA-20c reanalysis and possible sources of residuals in the AAM balance. Using these results, the performance of the reanalysis and the reliability of the terms of the AAM budget (Eq. 9) can be assessed. Secondly, the observed 20th century trends in the AAM and the torques are described (Sect. 4.2). In addition, these trends are linked to changes in the global atmospheric circulation observed in both this study and in literature.

4.1 Balance closure

Although AAM should be conserved, residuals in the calculated AAM balance can be expected, predominatly as a result of the assimilation of observations (Berrisford et al., 2011). In this section, first the AAM balance is given as calculated from the 3-hourly forecast data, in which case the tendencies are not yet affected by the assimilation of observations. Subsequently, the monthly AAM balance as calculated from the analysis data is given. Last, the temporal evolution of the balance residuals and the number of assimilated observations are described.

4.1.1 Forecast balance

In the forecast dataset, there is a clear correlation between the monthly mean AAM tendency and the monthly mean total torque (Fig. 4). The total torque is the sum of the mountain, the friction and the gravity wave torque. A negative total torque implies that there is a net AAM transport from the atmosphere to the earth, which corresponds to a negative tendency. The similar temporal evolutions of the tendency and torque could be expected, since conservation of AAM implies that the both terms are equal (Eq. 9). However, there is a small bias between both terms, because the torque is on average slightly lower than the tendency (Fig. 4). Even in the forecast data, the AAM balance is thus not perfectly closed, but has a small positive mean balance residual of about $3.66 \cdot 10^{18}$ kg m^2 s^{-2}. The temporal variability of the bias, which occurs mainly on an annual and biannual time scale, is considerably smaller than the variability of the tendency and the torques. On longer, multi-annual, time scales, the bias is approximately constant as it shows no clear trend within each 16-year period.

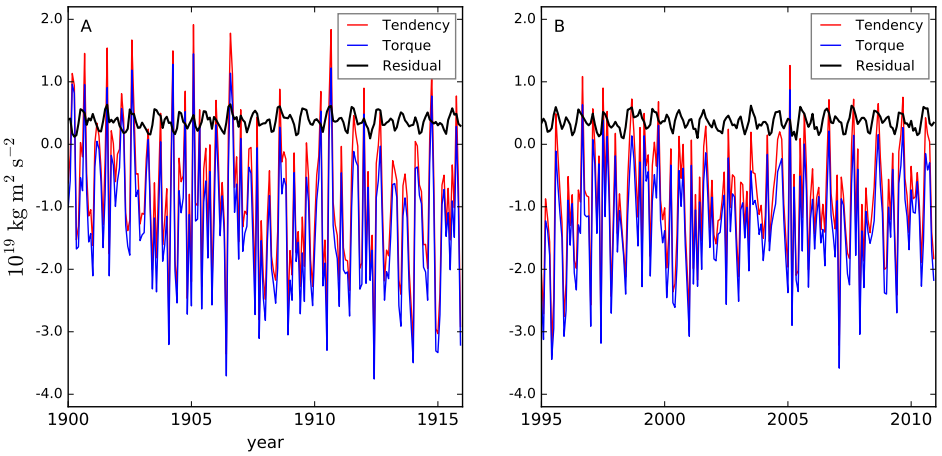

Figure 4: Monthly means of the 3-hourly AAM tendency, the total torque and the balance residual (tendency - torque) against time, for the periods 1900-1916 (A) and 1995-2010 (B)

Moreover, the biases in both the time periods 1900-1916 (Fig. 4A) and 1995-2010 (Fig. 4B) are very similar. This supports the assumption that the balance residual in the forecast data does not change throughout the 20th century, and therefore justifies the use of only the first and last 16 years of the data period to study the AAM balance in the forecasts.

The residuals in the AAM balance may be partly attributed to numerical approximations in the calculation of the different terms of the AAM budget, or to the horizontal interpolation of the data (Trenberth, 1995) to the regular latitude-longitude grid used in this study. Additionally, as suggested by Berrisford et al. (2011), the actual 3-hourly mean surface pressure may differ from the surface pressures available at each 3-hourly time step. This can result in errors in the mountain torque and thus a residual in the AAM balance. As shown in Figure 4, the monthly means of the tendency and the torque are predominantly negative. The mean tendency is $-8.57 \cdot 10^{18}$ kg m^2 s^{-2} in the period 1900-1916 and $-9.13 \cdot 10^{18}$ kg m^2 s^{-2} in the period 1995-2010. These mean tendencies are significantly larger than the tendencies fluctuating around zero observed by e.g. Berrisford et al. (2011) and Huang et al. (1999). This is an indication that the total torque is overestimated in the forecasts.

4.1.2 Analysis balance

The monthly AAM balance calculated from the analysis data (Fig. 5) closes much poorer than the balance in the forecasts (Fig. 4). The residuals are still predominantly positive, but on average they are considerably higher ($15.2 \cdot 10^{18}$ kg m^2 s^{-2}) and have a larger temporal variability than the residuals in the forecasts. These higher residuals are mainly caused by the change in the monthly AAM tendencies, in this case based on the differences in AAM between the beginning of consecutive months. The monthly tendencies are still on the same order of magnitude as in the forecasts, but the temporal average of the AAM tendency is much closer to zero ($-8.35 \cdot 10^{15}$ kg m^2 s^{-2}) than in the forecast balance, whereas the total torque is approximately the same. This differences in mean AAM tendency between the analysis and forecast data is most likely caused by the assimilation of observations, i.e. the adjustment of the forecasted surface pressure and wind fields to better match observations (Berrisford et al., 2011). Since this assimilation is not constrained to conserve mass or angular momentum (Berrisford et al., 2011), it can easily result in the poorly closed AAM balance. Nevertheless, it can be assumed that the tendencies in the analysis data are more realistic, since the analysis data are closer to the observations than the forecasts due to the assimilation. This assumption also implies that the model forecasts are considered to be inaccurate, which, together with the large imbalance in the analysis data, reduces the reliablity of the trend analysis.

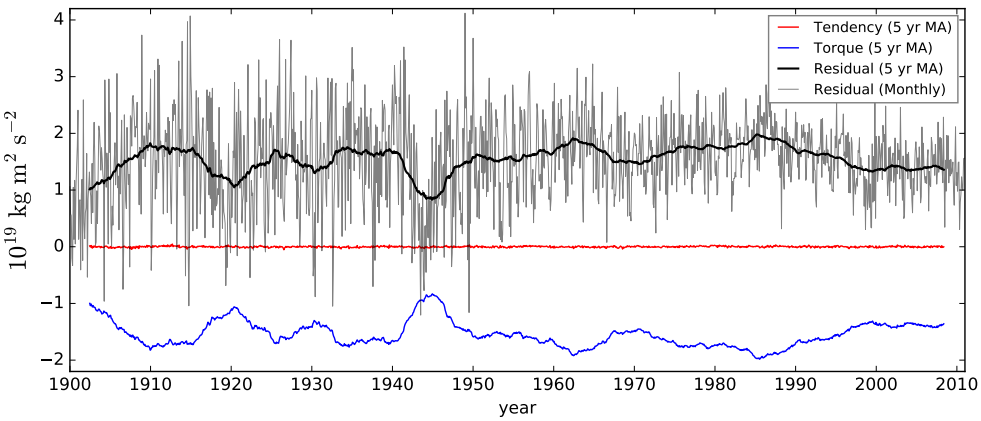

Figure 5: Full time series of the monthly balance residual and 5 year moving averages (MA) of the AAM tendency, torques and balance residuals during the complete 20th century, based on the analysis dataset.

The parameterized torques are not influenced by the assimilation and should thus be equal in both the analysis and the forecast data. The monthly means of the gravity wave and friction torque are indeed found to be approximately the same in both datasets. A small difference was observed, however, which is presumably related to the temporal overlap of consecutive forecasts at 9 UTC. The mountain torque, on the other hand, can be affected by the assimilation of pressure observations, because it is related to the global surface pressure distribution. In the analysis data, the mean mountain torque is stronger, or more negative, than in the forecast data: in the period 1900-1916 it is $-5.46 \cdot 10^{18}$ kg m^2 s^{-2} in the forecast data and $-7.18 \cdot 10^{18}$ kg m^2 s^{-2} in the analysis data; in the period 1995-2010 it is $-2.16 \cdot 10^{18}$ kg m^2 s^{-2} in the forecast and $-3.43 \cdot 10^{18}$ kg m^2 s^{-2} in the analysis. Compared to the differences in the tendency and balance residuals between the forecast and analyis, however, this difference in mountain torque is relatively small.

The predominatly negative mean torque and positive mean balance residuals in the analysis data are a clear indication that on average the torques are overestimated in the model. That is, more angular momentum is extracted from the atmosphere in the model than according to the observations. Such overestimated torques have also been observed in other reanalysis data sets by several studies (e.g. Madden and Speth, 1995; Huang et al., 1999; Berrisford et al., 2011). It does suggest, however, that the magnitude of the torque trends in the 20th century may not be very reliable. A more qualitative assessment of the changes in the magnitudes and zonal distributions of the individual torques may nevertheless still be of interest.

4.1.3 Temporal evolution

As shown in Figure 5, there is no significant long-term improvement in the closure of the AAM balance. This indicates that the strong increase in the number of assimilated observations during the 20th century (Fig. 6) has not improved the conservation of angular momentum in the reanalysis. The consistently large balance residuals also suggest errors the forecast model, causing the predicted atmospheric state to deviate from the observed atmospheric state in each forecast. The balance residuals have even increased on average with a linear trend of about $1.97 \cdot 10^{16}$ kg m^2 s^{-2} per year, or about $5 \cdot 10^{22}$ kg m^2 s^{-1} per year for the monthly integrated residual. However, the temporal variability of the residuals has decreased during 20th century (Fig. 5), which indicates that the precision of the model in closing the AAM balance has improved.

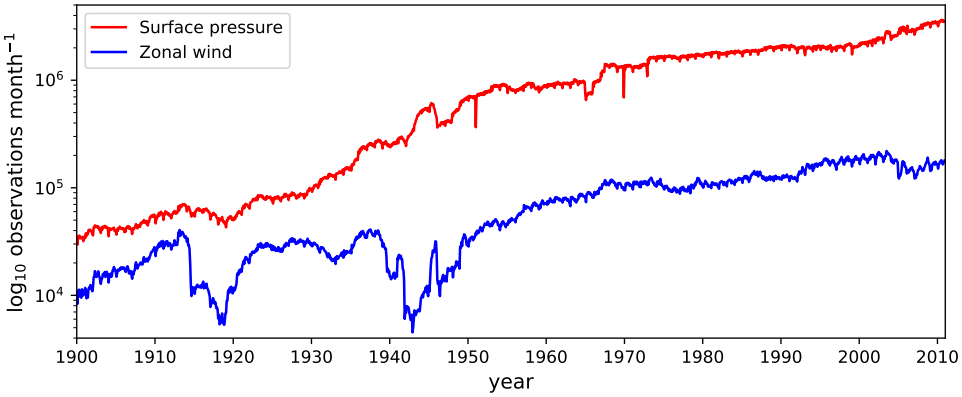

Figure 6: Total number of zonal wind and surface pressure observation observations assimilated each month for the ERA-20c reanalysis. See also Poli et al. (2016).

Interestingly, there are three clear minima in the magnitudes of the residuals during the first half of the 20th century, near 1900, 1920 and 1945 (Fig. 5). These lower residuals are mainly the result of the higher, less negative, torques in these periods. The timing of these lowest residuals corresponds roughly to the periods with the lowest number of assimilated wind observations (Fig. 6; Poli et al. (2016)). This connection suggests that long-term changes in the AAM budget observed in the data can be affected by changes in the number of assimilated observations.

4.2 Trend analysis

In this section, the results of the trend analysis are presented. First, the trends in the total AAM are given, followed by the changes in the Ω and relative AAM components. Additionally, these trends are linked to changes in air temperature and atmospheric circulation during the 20th century. Last, the trends in the mountain, gravity wave, and friction torques are described.

4.2.1 Total AAM

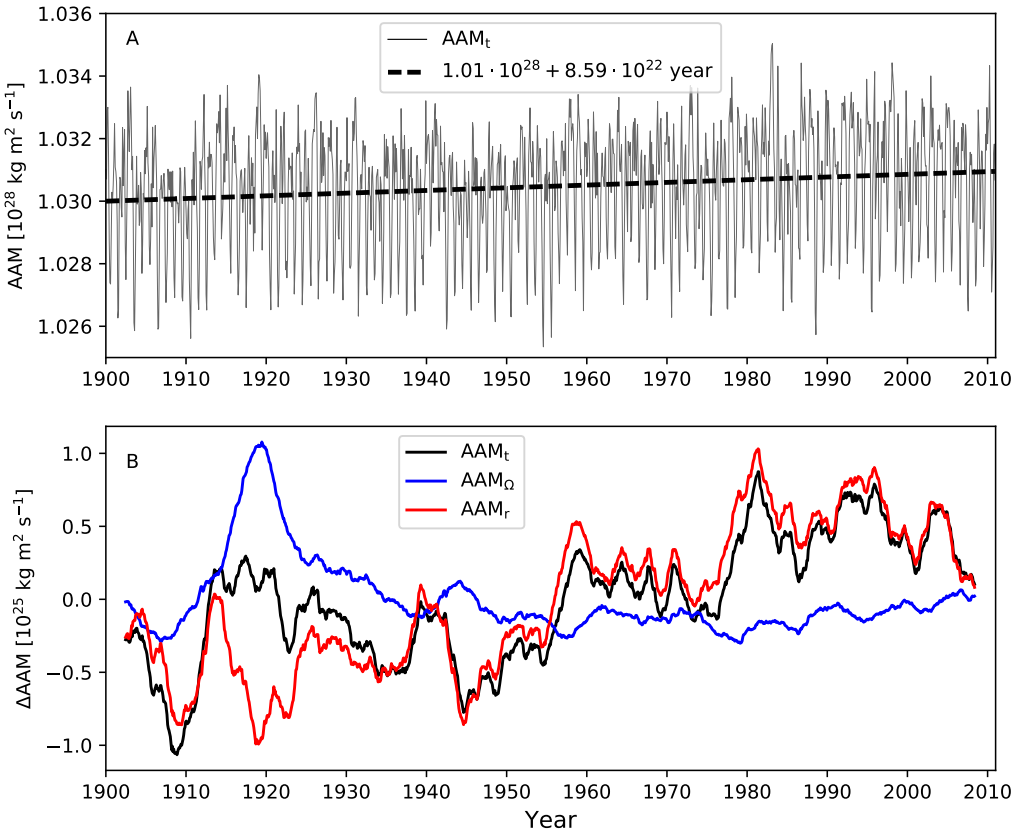

Figure 7: (A) The monthly means of the total AAM and its linear trend (thick dashed line) in the period 1900-2010 and (B) the 5-year moving averages of the anomalies of the total AAM (AAM_t) and its relative (AAM_t) and Ω (AAM_Ω) components

.

The total globally integrated AAM has a small positive linear trend during the 20th century of approximately $8.59 \cdot 10^{22}$ kg m^2 s^{-1} per year (Fig. 7A), which amounts to an increase of about $9.53 \cdot 10^{22}$ kg m^2 s^{-1} between 1900 and 2010. This increase is significantly smaller than the temporal mean and seasonal variations of the total AAM, but it is still significant. In the first decade and in the second half of the 20th century, the temporal evolution of the total and relative AAM anomalies are very similar (Fig. 7B). This similarity shows that the total AAM trend is mainly due to an increase in its relative component. Around 1920, however, the total AAM deviates clearly from the relative AAM (Fig. 7B), which is due to a large positive Ω-AAM anomaly in this period.

4.2.2 Ω-AAM

The Ω-AAM component (Eq. 7) is due to the rotation of the atmosphere along with the rotation of the earth. The time series of the Ω-AAM component (Fig. 7B) has a negative linear trend of about $0.32 \cdot 10^{23}$ kg m^2 s^{-1} per year. However, given the peak in Ω-AAM around 1920, this linear trend is assumed to be of little value. The large Ω-AAM peak is surprising, because the mass of the atmosphere should be approximately constant in time (Berrisford et al., 2011). Variations in Ω-AAM may be due to changes in the atmospheric water content or changes in the meridional redistribution of the dry mass of the atmosphere (Madden and Speth, 1995). The dry atmospheric mass is obtained by substracting the globally integrated total column water from the total mass of the atmosphere (e.g. Berrisford et al., 2011). The total mass of water in the atmosphere is over two orders of magnitude smaller than the dry atmospheric mass (Fig. 8). It is not significantly larger around 1920 (Fig. 8) and has therefore not contributed to the Ω-AAM peak. Nevertheless, the atmospheric water content has increased significantly during the 20th century (Fig. 8), which results in a linear trend in angular momentum of approximately $0.19 \cdot 10^{23}$ kg m^2 s^{-1}.

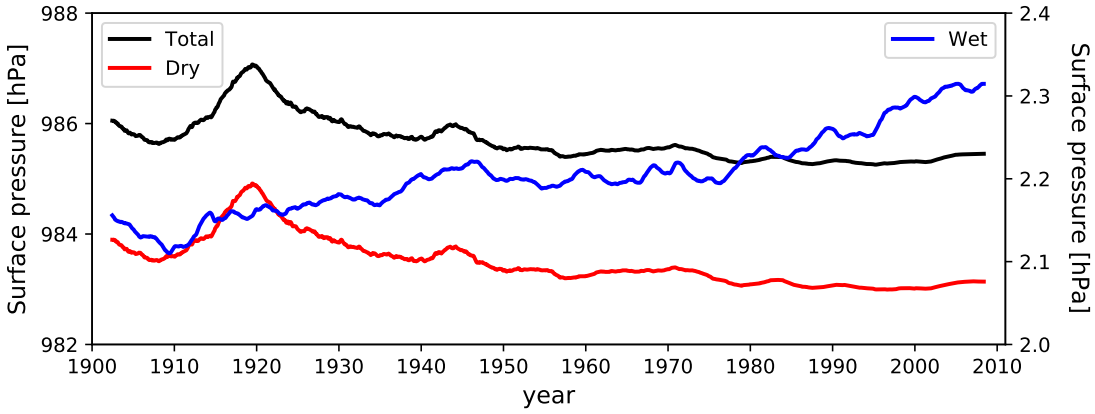

Figure 8: 5 year moving averages of the global mean surface pressure (Total; left y-axis) and the contributions of the dry atmospheric mass (Dry; left y-axis) and the atmospheric water content (Wet; right-axis) to the surface pressure.

The time series of both the global mean total and the dry surface pressures show a similar peak around 1920 (Fig. 8). This indicates that the high Ω-AAM anomaly in this period is mostly due to a spurious peak in the dry surface pressure. To understand this peak, it is interesting to study the meridional distribution of the evolution of the surface pressure in the 20th century. At all latitudes, the surface pressure in the period around 1920 is higher than the temporal mean surface pressure (Fig. 9). This indicates that the 1920 peaks in dry surface pressure and Ω-AAM are mainly a global issue. The surface pressure anomalies around 1920 are largest at higher latitudes, especially in the southern hemisphere (Fig. 9), although the contribution of the higher latitudes to the Ω-AAM peak is relatively low (Eq. 8).

Apart from the peak around 1920, two long-term surface pressure trends can be deduced from Figure 9. In both the Arctic and Antarctic regions, the surface pressure has decreased throughout the 20th century, whereas it has increased around 40° S. As shown by Hines et al. (2000) in another reanalysis, the surface pressure trend in the Antartica region may largely be considered an artifact from the increased number of assimilated observations (Fig. 6; Poli et al. (2013)). Changes in the availability of observations are also assumed to be the cause of the 1920 peak in surface pressure, which is not physically realistic as the dry atmospheric mass should be approximately conserved. Trenberth and Smith (2005) estimated that surface pressure variations due to changes in the composition of the atmosphere are on the order of 0.01 hPa, which is insignificant compared to the observed surface pressure anomalies (Fig. 8, 9).

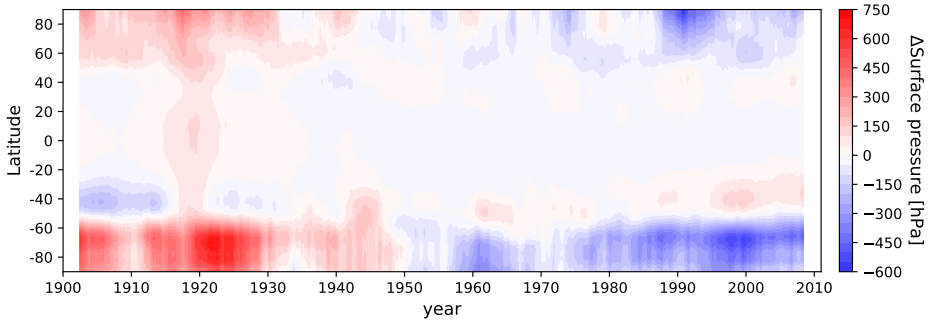

Figure 9: Latitude-time distribution of anomalies of the zonal mean surface pressure with respect to the temporal mean surface pressure at each latitude. Shown are the 5-year moving averages of the anomalies.

4.2.3 Relative AAM

The relative AAM component (Eq. 6) has increased with a linear trend of about $1.18{\cdot}10^{23}$ kg m^2 s^{-1} during the 20th century. This trend amounts to gain in relative AAM of about $1.29{\cdot}10^{25}$ kg m^2 s^{-1}, an increase of approximately 10%. Since the relative AAM component is related to the magnitude and meridional distribution of the zonal winds, we study the latitude-height distribution of the trends in relative AAM (Fig. 10A) and zonal winds (Fig. 10B) in more detail.

A major contribution to the global relative AAM trend comes from the tropical upper-troposphere, roughly between 20°S and 20°N, and the lower stratosphere. This is associated with an increase in zonal wind speed of about 4 m s^{-1} in this region (Fig. 10B) in the 20th century. In part of the equatorial stratosphere (≈ 20-50 hPa), however, the relative AAM has a strongly negative trend, corresponding to a decrease in zonal wind speed of up to 15 m s^{-1}. In the mid-latitudes, between approximately 20° and 40° in both hemispheres, the relative AAM has decreased over the whole depth of the troposphere (Fig. 10A). Further poleward, roughly between 40° and 60° in both hemispheres, the relative AAM has increased, both in the troposphere and the lower stratosphere. These negative and positive relative AAM trends in the mid-latitudes correspond to a decrease and increase in zonal wind, respectively, and are strongest in the southern hemisphere. This pattern suggests that in the mid-latitude troposphere, the relative AAM is primarily redistributed to higher latitudes. The different magnitudes of the mean and the maximum trends also indicate this redistribution: the mean relative AAM trend, averaged over all latitudes and model levels (Fig. 10A), is about $6.4{\cdot}10^{13}$ kg m s^{-1} per year. In contrast, the strongest trends in the mid-latitudes have a magnitude on the order of $1{\cdot}10^{15}$ kg m s^{-1}, which is about 15 times higher than the mean trend.

As shown in Figure 10A, the maximum increase in zonal winds is located in the stratosphere (≈100 hPa) around 60° S. However, this maximum does not correspond with the strongest relative AAM

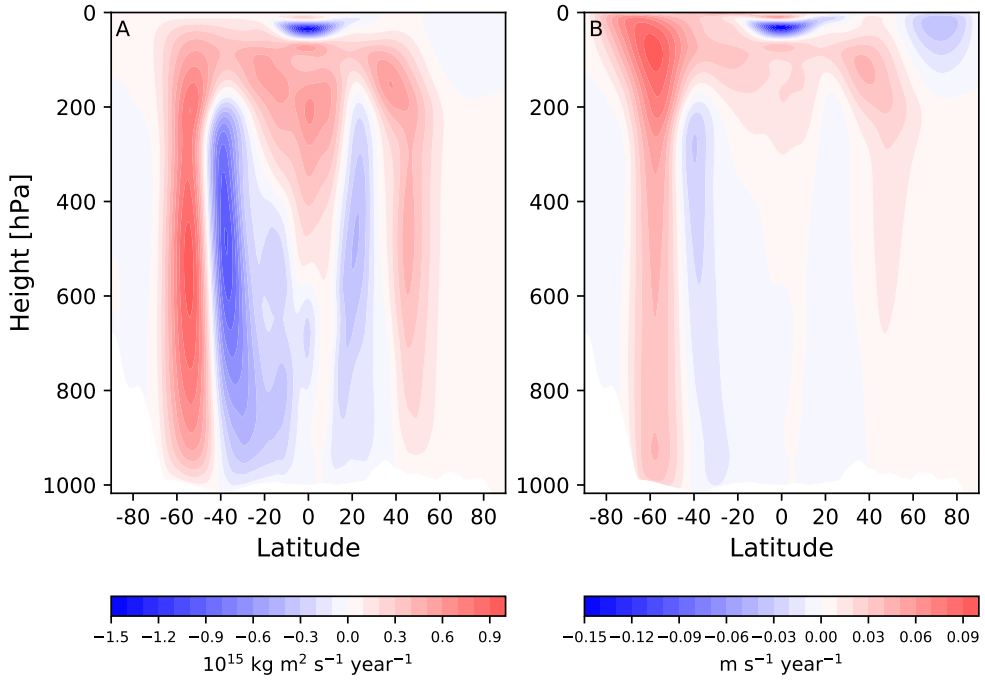

Figure 10: Linear trends during the 20th century of the relative AAM (A) and the zonal wind (B) at all available latitudes and 91 model levels. For plotting purposes, the model levels have been converted to pressure levels using the zonal and temporal mean surface pressures (ECMWF, 2013)

trend (Fig. 10B), which is because of the smaller layer depths represented by the higher model levels. Similarly, the decreasing zonal winds in the stratosphere around 80° N do not correspond to a large decrease in relative AAM. This difference is augmented by the rapid decrease in radius ($a \cos \phi$) at high latitudes.

The trends in the relative AAM and zonal wind distribution can be related to the changes in air temperatures during the 20th century (Fig. 11A). The temperature has increased in most of the troposphere, with the highest trends in the mid-latitudes in the southern hemisphere and tropical upper-troposphere. The temperatures have decreased in most of the lower stratosphere, especially at high latitudes in the southern hemisphere. In part of the arctic stratosphere, however, the temperature has increased, although not directly above the tropopause. The temperature increase in the troposphere and decrease in the stratosphere can be related to the increasing CO_2 concentrations (IPCC, 2013). The strong temperature decrease in the stratospheric can also be attributed to the declining ozone concentrations (e.g. Ramaswamy et al., 2001; IPCC, 2013). Following the definition by WMO (1957) and using the algorithm described by Reichler et al. (2003), the tropopause is determined as the first height at which the temperature decreases with less than 2 K km^{-1}. The observed changes in temperature (Fig. 11A) result in a stronger meridional temperature gradient across the tropopause (Chen and Held, 2007), especially in the mid-latitudes, where the tropopause height lowers quickly with latitude (Fig. 11B). As shown in Figure 11B, the 20(30)-year mean tropopause height has risen by approximately 5 hPa in the tropics during the 20th century. Assuming hydrostatic equilibrium and an air density of 0.2 kg m^{-3}, this rise corresponds to approximately 250 m. This increase in tropopause height is likely a consequence of warming below and cooling above the tropopause (Fig. 11A) (Seidel

and Randel, 2006; Yin, 2005; Lorenz and DeWeaver, 2007). Remarkable is the strong tropopause rise in the southern hemisphere at high latitudes, presumably because the decrease in stratospheric temperatures is strongest in this region. Several studies have already that both the stronger temperature gradient and the higher tropopause can result in stronger and more poleward jet streams and mid-latitude westerlies (Lorenz and DeWeaver, 2007; Chen and Held, 2007; Yin, 2005). The increase and poleward redistribution of relative AAM in the mid-latitudes can thus be related to the increasing CO_2 and decreasing ozone concentrations.

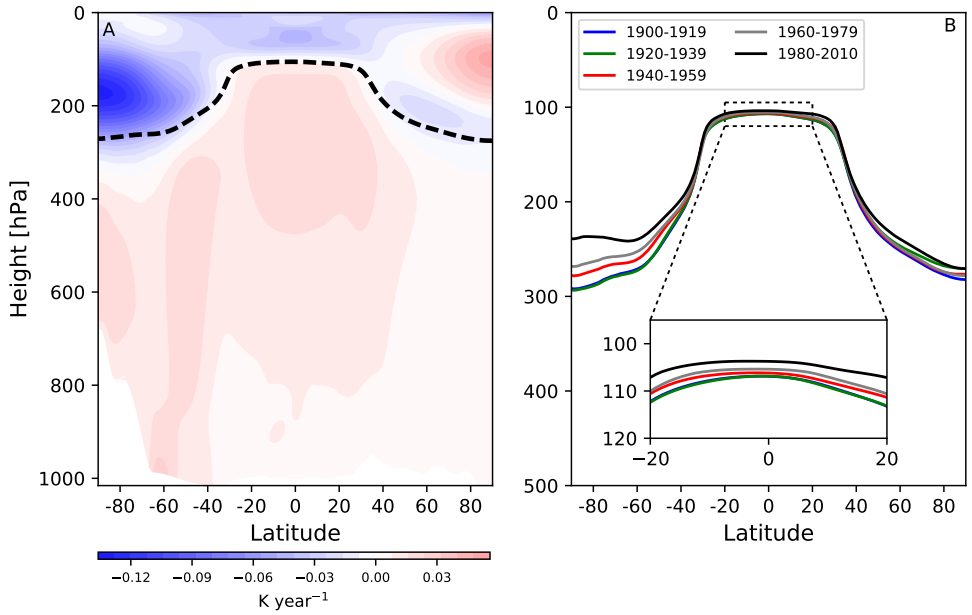

Figure 11: A: Linear trends during the 20th century of air temperature AAM at all available latitudes and 91 model levels, again converted to pressure levels as in Figure 10. B: meridional distribution of the mean tropopause height, calculated from the 20(30)- year mean temperatures in each 20(30)year period. The black dashed line (A) is the mean tropopause height in the 20th century

4.2.4 Torques

Since angular momentum is a conserved quantity, the positive AAM trend (Sect. 4.2.1) should be the result of a positive mean total torque throughout the 20th century. As was shown in Section 4.1, this is not found as the total torque is negative on average. Given the meridional shifts in relative AAM and zonal winds in the mid-latitudes, it is nevertheless interesting to study the changes in the mountain, friction and gravity wave torques relative to each other.

The globally integrated gravity wave torque has a small negative linear trend of about $1.0{\cdot}10^{16}$ kg m^2 s^{-1} per year and has little variability on multi-annual time scales (Fig. 12A). On average, the friction torque has decreased as well, by about $4.1{\cdot}10^{16}$ kg m^2 s^{-1} per year. The mountain torque, on other hand, has increased by about $3.2{\cdot}10^{16}$ kg m^2 s^{-1} per year. The global friction torque has thus become stronger, extracting more angular momentum from the atmosphere, whereas the mountain torque has become weaker. This indicates that the relative importance of the friction torque in the total torque has increased in the 20th century. However, both the friction torque and the mountain torque have a large multi-annual variability (Fig. 12A), which may at least partly by attributed to changes in the number of assimilated observations throughout the 20th century, as was mentioned in Section 4.1.3.

The meridional distribution of the trends in the zonally integrated torques (Fig. 12B) has a similar pattern as the zonal wind and relative AAM trends (Fig. 10) near the surface. In both hemispheres, the torques have increased in the subtropics and the lower mid-latitudes. Further poleward in the mid-latitudes, the torques have increased, around 55° in the southern hemispere and 45° in the northern hemisphere. This pattern suggests that the regions with the most negative torques have shifted poleward, corresponding to the poleward redistribution of relative AAM. This makes sense, because the sign and magnitude of the torques are dependent on the direction and strength of the zonal winds (ECMWF, 2013), so stronger zonal winds will result in stronger torques.

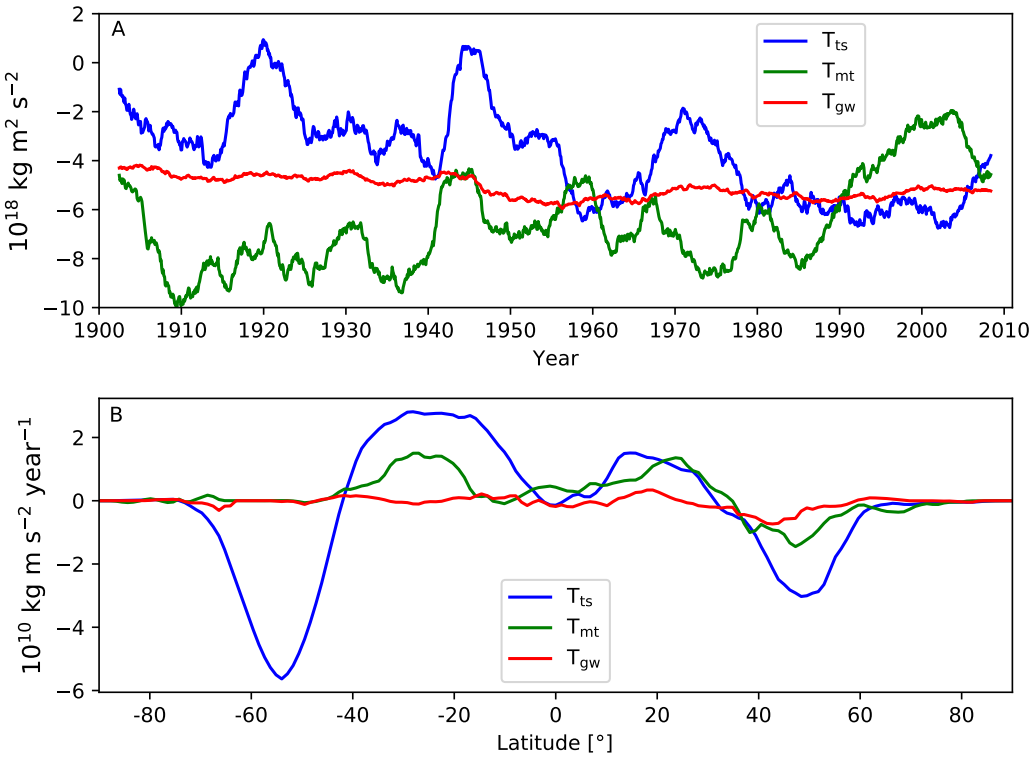

Figure 12: A) 5-year moving averages of the friction (turbulent stress) torque (T_{ts}), the mountain torque (T_{mt}) and the gravity wave torque (T_{gw}) and B) 20th century trends of the zonally integrated T_{ts}, T_{mt} and T_{gw} per latitude.

This poleward shift in torques has presumably also resulted in the change in the contributions of the mountain torque and friction torque (Fig. 12A). In the southern hemisphere, both the mountain and friction torque have increased in the lower mid-latitudes (≈ 20°-40°), whereas farther poleward (≈ 55°) only the friction torque has decreased significantly. Around approximately 15°-30° the northern hemisphere, the increase in mountain torque is similar to the increase in friction torque, but around 50° the friction torque has decreased significantly more than the mountain torque.

This shift from mountain torques to friction torques can be considered a result of the shift of the mid-latitude westerlies latitudes with less orography (Fig. 13A). This is most clear in the southern hemisphere, where mainly the Andes can contribute greatly to the mountain torque around 20°-40° (e.g. Weickmann et al., 1997; Iskenderian and Salstein, 1998). The increasing mountain torque in the

southern hemisphere may therefore be associated with the small decrease in surface pressure west of the southern part of the Andes, as well as the lower zonal pressure gradient across southern Africa (Fig. 13B). There is little orography and mainly ocean around 60° latitude in the southern hemisphere and therefore little change in mountain torque in response to the changes in surface pressure at this latitude. In the northern hemisphere, the increased mountain torque in the lower latitudes may be related to the decreasing surface pressures west of the Rocky Mountain, over north-west Africa and over India and the higher surface pressure over the Himalaya (Fig. 13). The decreasing mountain torque at higher latitudes is likely due to the lower surface pressure over the northern part of the Rocky Mountains and eastern Siberia.

In both hemispheres, the 20th century trends in zonal wind speed near the surface have been strongest over the oceans (Fig. 14A). Since surface drag over water surface only results in friction torque, this can explain why the friction torques have changed most. The relatively constant gravity wave torque may also be related with the spatial distribution of the zonal wind trends. In most of the continental areas where the zonal wind has changed considerably, e.g. Africa and Australia, the standard deviation of the orography is relatively low (Fig. 14B). This standard devation is a measure of the subgrid-scale orography, an important parameter in the parameterization of the gravity wave drag (ECMWF, 2013). In the regions with most subgrid-scale orography, e.g. the Himalayas and the Andes (Fig. 14B), the zonal wind speeds have barely changed (Fig. 14A).

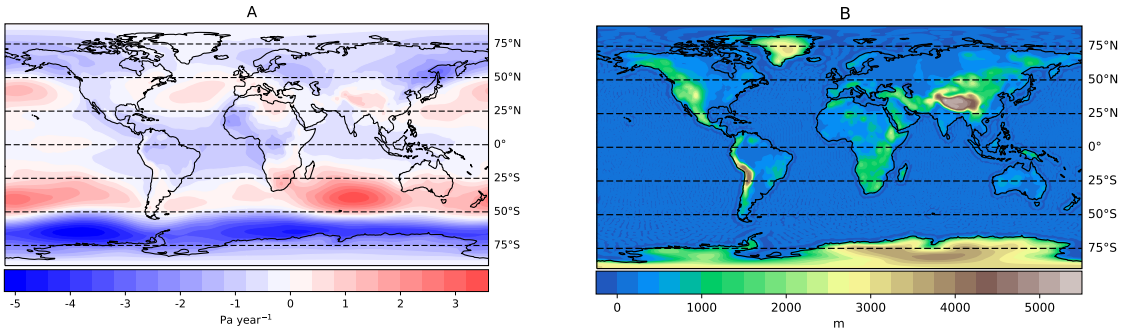

Figure 13: (A) Spatial distribution of the linear trends in surface pressure trends, area-weighted by multiplying with $\cos\phi$, and (B) the height of the orography used for ERA-20c

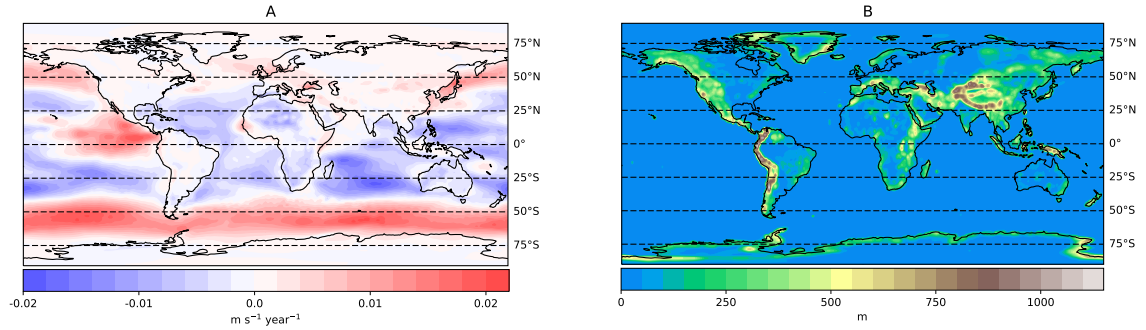

Figure 14: (A) Spatial distribution of the linear trends in zonal wind at the lowest model level, area-weighted by multiplying with $\cos\phi$, and (B) the standard deviation of the orography in ERA-20c as a measure of the sub-grid scale orography

5 Discussion

In this section, the methodology and the results of this study and the interpretation of the results are discussed and compared with literature. The structure of this discussion is similar to the results (Sect. 4). The results regarding the closure of the AAM balance in the forecast and analysis data are discussed in Section 5.1. The trends in the AAM budget and their interpretation are discussed in Section 5.2

5.1 Balance closure

The closure of the AAM balance in the ECMWF ERA-20c reanalysis was studied using both the 3-hourly forecast and the monthly mean analysis data. Because no tendencies were calculated between consecutive forecasts, the AAM balance in the forecast data is not affected by the assimilation of observations (Poli et al., 2013). A balance residual close to zero can thus be expected in the forecasts, especially since part of the numerical schemes is designed to be angular momentum conserving (ECMWF, 2013; Simmons and Burridge, 1981). Nevertheless, a small positive bias was found in the AAM balance, because the mean total torque is slightly more negative than the mean tendency, which shows that angular momentum is not conserved in the forecasts. The closure of the AAM balance in the forecast data has only been determined for the periods 1900-1916 and 1995-2010, because it was assumed to be constant on a multi-annual time scale. Despite the biannual and annual variability, the residuals show no long-term trend (Fig. 4), so this assumption holds.

Part of the bias may be attributed to several numerical approximations in the retrieval and use of the data. Upon retrieval from the ECMWF data server, the data are automatically interpolated horizontally from their original T159 spectral resolution (Poli et al., 2016) to the regular latitude-longitude grid used in this study. Such changes in coordinate system and resolution have been found to result in errors in the conservation of e.g. energy (Hennermann, 2017) and mass (Trenberth, 1991) in data. Numerical errors may also arise from the calculation of the horizontal integrals (Eq. 8) or zonal gradients (Eq. 9). This error could be reduced by using the data on their original spectral resolution. Part of the bias could also caused by an overestimation of the calculated mountain torque (Berrisford et al., 2011). The mountain torque is based on the 3-hourly instantaneous surface pressures, which may differ from the mean surface pressure in each 3-hour time period (Berrisford et al., 2011), since the time step in the model itself is 0.5 hour (Poli et al., 2016).

The balance residual in the analysis data, on the other hand, is significantly larger and more variable than in the forecast data. The mean monthly tendency in the analysis data is closer to zero than in the forecasts data, whereas the mean total torque has not changed significantly (Figs. 4,5). This indicates that the imbalance in the forecasts is caused by an overestimation of the torques. The mean balance residual in the analysis is about $15.2 \cdot 10^{18}$ kg m^2 s^{-2}, which is comparable to residuals found by other studies: Berrisford et al. (2011) found a mean balance residual of about $15 \cdot 10^{18}$ kg m^2 s^{-2} between 1989 and 2002 in the ECMWF ERA-40 reanalysis, and a mean balance residual of about $7 \cdot 10^{18}$ kg m^2 s^{-2} between 1989 and 2008 in the more recent ERA-Interim. Madden and Speth (1995) found a mean negative bias of approximately $15.2 \cdot 10^{18}$ kg m^2 s^{-2} in reanalysis data over a period of 13 months. In a 29-year period reanalysis data set, Huang et al. (1999) found a mean negative residual of about $10.9 \cdot 10^{18}$ kg m^2 s^{-2}.

Further studying the contribution of the different torques to the residuals can provide directions for further model improvement (Huang et al., 1999; Madden and Speth, 1995). Around 1920 and 1940, the balance residuals are significantly lower (Fig. 5). The lower residuals around 1920 correspond approximately to an increase in the friction torque and the lower residuals around 1940 correspond to an increase of both the mountain and friction torque (Fig. 12). This suggests that the balance residual can be attributed to an overestimation of both the mountain and the friction torques. An

overestimated friction torque was also observed by Madden and Speth (1995). On the other hand, Huang et al. (1999) found that the balance residuals were mainly because the gravity wave torque was too strong. Interestingly, the gravity wave torque in this study is weaker than found by Huang et al. (1999), whereas the mountain torque is much stronger. Part of this shift between the gravity wave and mountain torque may be due to a differences in horizontal resolution and thus the scales of orography that can be resolved (Brown, 2004). The sum of the mountain and gravity wave torque is higher here than in the study of Huang et al. (1999), which contributes to the larger balance residual.

A decrease of the residuals in time is an indication of improvements in model performance. Berrisford et al. (2011) found that in both ERA-40 and ERA-Interim, the annual mean balance residuals have decreased since 1989. In this study, the residuals also decreases slightly between about 1990 and 2000 (Fig. 5), but throughout the whole 20th century there is no significant improvement in the closure of the AAM balance. In contrast, a positive linear trend of the balance residuals is observed, which is on the same order of magnitude as the trend in AAM and indicates that the negative trend in the total torque is overestimated. The less negative torque and thus lower balance residuals around 1920 and 1940 are presumably related to the decrease in the number of assimilated zonal wind observations in these periods (Fig. 6; (Poli et al., 2016)). This relation, in combination with the relatively large balance residuals and the use of only surface observations (Poli et al., 2016), suggests that reliability of the trend analysis might be questionable. It is therefore important to compare trends with literature as well as to assess their theoretical basis.

5.2 Trend analysis

To study trends in the AAM budget, the monthly mean AAM and the monthly mean torques were calculated throughout the 20th century. The linear increase in the total AAM found in this study is approximately $0.86 \cdot 10^{23}$ kg m^2 s^{-1} per year. In response to a doubling of the CO_2-concentration in about 60 years, Huang et al. (2001) observed an increase in AAM of approximately $2.4 \cdot 10^{23}$ kg m^2 s^{-1} per year. Averaged over 16 climate models, Räisänen (2003) found an increase in relative AAM of about $1.0 \cdot 10^{23}$ kg m^2 s^{-1} when the CO_2-concentration doubles in 70 years. Both increases are larger than the trend found in this study, which is not surprising because the CO_2 concentration has not doubled yet in the 20th century (IPCC, 2013). In reanalysis data, del Rio (1999) found an increase in the length of day of about $5.6 \cdot 10^{-5}$ s per year between 1949 and 1997, which corresponds to an AAM trend of approximately $3.3 \cdot 10^{23}$ kg m^2 s^{-1} per year (Rosen and Salstein, 1983). This trend is also significantly larger than the trend in this study, which may to some extent be explained by the shorter time period studied by del Rio (1999): as shown in Figure 7B, the AAM trend in the 2nd half of the 20th century is slightly larger than the trend over the whole 20th century. Using the NCAR/NCEP 20CR reanalysis data, Paek and Huang (2012) also found an increase in relative AAM between 1871 and 2008. Although they did not explicitly quantify the trend, it is on the same order of magnitude (Fig. 1a in Paek and Huang (2012)) as the trend in this study.

However, Paek and Huang (2012) also found that in the 2nd half of the 20th century, the relative AAM in 20CR was on average lower than in several other reanalysis data sets and had a different temporal evolution (Paek and Huang, 2012). The mean relative AAM in this study is higher than was found in 20CR by Paek and Huang (2012) and therefore more comparable to the other data sets, so presumably more accurate. However, the mean and temporal evolution of the AAM were not compared in detail with other data sets in this study, which should be subject for further research.

The AAM trend is mainly due to an increase of its relative component, which is related to the zonal winds. The main changes in relative AAM are an increase in the tropical upper-troposphere and a poleward redistribution in the mid-latitudes. A poleward shift of the relative AAM was also found by, and by Räisänen (2003) and Huang et al. (2001) in response to higher CO_2 concentrations. This shift is most likely due to the increase in tropospheric temperatures and decreasing in lower-stratospheric

temperatures, as found by several studies (e.g. Lorenz and DeWeaver, 2007; Chen and Held, 2007; Yin, 2005). These temperature changes can be associated with the decrease in ozone in the stratosphere as well as the increase in CO_2 in the troposphere (IPCC, 2013). The increase in relative AAM and zonal winds in the tropical upper-troposphere has also been observed by Huang et al. (2001) and Räisänen (2003) in response to increasing CO_2 concentrations and global warming. No definite explanation for this zonal wind increase has been found. However, it was suggested by Huang et al. (2001) that this increase may be due to an intensification of El-Niño's or the Madden-Julian Oscillations in response to global warming. Such an intensification has been found to result in stronger westerly winds in the tropical upper-troposphere (Lee, 1999). Another factor can be the tropical easterly jet that exists in South Asia (Koteswaram, 1958), since Abish et al. (2013) observed that this easterly jet has weakened 20th century, which gives an increase in the mean zonal wind.

The poleward redistribution of relative AAM near the surface has presumably also caused the poleward shift of the torques in the mid-latitudes. The torques are dependent on the zonal wind speed, thus such a shift was to be expected. The poleward shift of the torques led to a change in the contributions of the friction and mountain torques to the total torque. Especially in the southern hemisphere, the relative AAM decreases at latitudes with significant orography ($\approx 35^\circ$ S) and increass at latitudes with little orography ($\approx 55^\circ$ S), resulting in a weaker mountain torque. This implies that the relative importance of mountains in the atmospheric circulation decreases due to the poleward shift of the relative AAM.

The temporal evolution of the omega-term shows a spurious peak around 1920. This peak is caused by a global increase in surface pressure, mostly in the high-latitudes of the southern hemisphere. Since mass should be conserved, the peak is considered to be an artifact of the number of assimilated pressure observations and changes therein (Poli et al., 2016; Hines et al., 2000). Such spurious surface pressure changes can also influence the trends in the mountain torque, which depends on the zonal surface pressure distribution. Similarly, the strong increase in the number of assimilated zonal wind observations has likely also impacted the trends in the relative AAM. The absence of temperature and upper-air observations in the assimilation also lowers the reliabilty of the relative AAM trends in the upper-atmosphere (Poli et al., 2013, 2016), indicating the importance of comparing the trends to other data sets. Nevertheless, the similarities of the trends in angular momentum, zonal wind and temperature to trends reported by other studies and the theoretical basis of the trends indicate a sufficient significance of the results.

6 Conclusion

In this research, the angular momentum budget of the atmosphere in the period 1900-2010 has been studied using the ECMWF ERA-20c reanalysis. The total atmospheric angular momentum (AAM) has increased during the 20th century with a small, but significant, linear trend. This positive AAM trend is mostly associated with an increase in the relative AAM component, which is related to the zonal wind distribution. The main changes in the relative AAM are an increase in most of the stratosphere and the tropical upper-troposphere, as well as a poleward redistribution in the mid-latitudes. These changes are mainly attributed to the tropospheric warming and the cooling in the lower stratosphere, most likely associated with the rising CO_2-levels and a decrease in stratospheric ozone (IPCC, 2013). The AAM trend can thus be understood as a result of the global warming in the 20th century (IPCC, 2013). This is supported by the AAM changes in response to e.g. higher CO_2-concentrations observed in other studies (Räisänen, 2003; Huang et al., 2001; Paek and Huang, 2013, 2012).

The total torque, the earth-atmosphere exchange of angular momentum, has increased in the tropics and subtropics and decreased in the mid-latitudes. This patterns is viewed as a poleward shift of the westward (negative) torques in the mid-latitudes, caused by the redistribution of the relative AAM to higher latitudes. The poleward shift in torques is accompanied by an increasing contribution of the friction torque to the total torque. This is partly interpreted as a result of the shift of the dominant westerlies to higher latitudes with less orography, but it is also because the zonal wind trends are strongest over the ocean. The relatively stronger friction torque indicates that the contribution of orography in maintaining the mid-latitude AAM balance has decreased.

Unlike the relative AAM, the omega (Ω)-AAM component, which accounts for the rotation of the atmosphere along with the earth, did not have a clear trend. Around 1920, the Ω-AAM was significantly larger than in the rest of the 20th century. This peak can be explained by neither a rapid increase in atmospheric moisture content nor a strong equatorward redistribution of the atmospheric mass. The anomalously high Ω-AAM and global mean surface pressures around 1920 are therefore considered to be an artifact of the low and rapidly changing amount of assimilated observations (e.g. Poli et al., 2016; Hines et al., 2000).

The closure of the AAM balance was determined to assess the ability of ERA-20c to conserve angular momentum, which is considered a measure of model performance and the reliability of the trends. In the forecasts, the AAM balance is not closed, but the residuals are small compared to the torques and approximately constant on multi-annual time scales. The monthly residuals in the analysis data, however, are considerably higher and more variable in time. Althought the analysis data fits the observations better than the forecasts (Poli et al., 2013), the larger imbalance reduces the reliability of the trends. These large residuals are mainly attributed to inaccuracies in the torques, because the global torque is on average not near zero but strongly negative. It should thus be noted that the exact magnitudes of the trends in the different torques are uncertain. Despite the increasing number of assimilation observations, no clear improvement of the closure of the AAM balance throughout the 20th century was observed. This is attributed to errors in the forecast model and also indicates that the uncertainty in the trend analysis due to the large imbalance has not decreased during the 20th century. Furthermore, it is found that the temporal evolutions of the AAM balance residuals and the amount of assimilated zonal wind observations are quite similar, especially in the first half of the 20th century. Since the changes in the balance residual are mainly due to changes in the total torque, it is very likely that the torque trends have been affected by changes in the number of observations.

Such a connection with the amount of assimilated observations has likely also influenced the magnitude of the trends in zonal wind, the relative AAM, and temperature (Poli et al., 2013). Given the large increase in the number of weather observations throughout 20th century (Poli et al., 2013), this issue is probably hard to overcome completely in long reanalysis data series. Nevertheless, the

large residuals in the AAM balance suggests that improving the parameterizations of the gravity wave and turbulent stress drag may increase the reliability of the trends in the AAM budget. To verify the significance of the 20th century trends, it is also recommended for further research to compare in detail the AAM trends found in ERA-20c to trends in the AAM budget of other reanalysis data sets.

Acknowledgements

I thank my supervisor Chiel van Heerwaarden for his supervision during my master thesis. The weekly meetings to discuss my progress were very useful to better understand and interpret my results, to get advice and ideas on how to proceed, and occasionally to regain some motivation. Furthermore, I acknowledge the European Centre for Medium-Range Weather Forecasts for the availability of the ERA-20c reananalysis data on their data server.

References

Abarca del Rio, R., D. Gambis, and D. A. Salstein, 2000: Interannual signals in length of day and atmospheric angular momentum. *Ann. Geophys.*, **18 (3)**, 347–364, doi:10.1007/s00585-000-0347-9.

Abish, B., P. V. Joseph, and O. M. Johannessen, 2013: Weakening trend of the tropical easterly jet stream of the boreal summer monsoon season 1950–2009. *J. Climate*, **26 (23)**, 9408–9414, doi:10.1175/JCLI-D-13-00440.1.

Anderson, J. R., and R. D. Rosen, 1983: The latitude-height structure of 40–50 day variations in atmospheric angular momentum. *J. Atmos. Sci.*, **40 (6)**, 1584–1591.

Beljaars, A. C. M., A. R. Brown, and N. Wood, 2004: A new parametrization of turbulent orographic form drag. *Quart. J. R. Meteor. Soc.*, **130 (599)**, 1327–1347, doi:10.1256/qj.03.73.

Berrisford, P., P. Kållberg, S. Kobayashi, D. Dee, S. Uppala, A. J. Simmons, P. Poli, and H. Sato, 2011: Atmospheric conservation properties in ERA-Interim. *Quart. J. R. Meteor. Soc.*, **137 (659)**, 1381–1399, doi:10.1002/qj.864.

Brown, A. R., 2004: Resolution dependence of orographic torques. *Quart. J. R. Meteor. Soc.*, **130 (603)**, 3029–3046, doi:10.1256/qj.04.21.

Chao, B. F., 1989: Length-of-day variations caused by El Niño-Southern Oscillation and Quasi-Biennial Oscillation. *Science*, **243 (4893)**, 923–925, doi:10.1126/science.243.4893.923.

Chen, G., and I. M. Held, 2007: Phase speed spectra and the recent poleward shift of Southern Hemisphere surface westerlies. *Geophys. Res. Lett.*, **34 (21)**, L21 805, doi:10.1029/2007GL031200.

Compo, G. P., and Coauthors, 2011: The Twentieth Century Reanalysis Project. *Quart. J. R. Meteor. Soc.*, **137 (654)**, 1–28, doi:10.1002/qj.776.

del Rio, R. A., 1999: The influence of global warming in earth rotation speed. *Ann. Geophys.*, **17 (6)**, 806–811, doi:10.1007/s00585-999-0806-x.

ECMWF, 2013: *Part III: Dynamics and Numerical Procedures*. IFS Documentation, ECMWF, operational implementation 19 June 2012.

Hennermann, K., 2017: ERA-Interim: What is the spatial reference. URL https://software.ecmwf.int/wiki/display/CKB/ERA-Interim%3A+What+is+the+spatial+reference.

Hersbach, H., P. Poli, and D. Dee, 2015: 18. The observation feedback archive for the ICOADS and ISPD data sets. ECMWF ERA report series no. 14, 31 pp.

Hines, K. M., D. H. Bromwich, and G. J. Marshall, 2000: Artificial surface pressure trends in the NCEP–NCAR reanalysis over the Southern Ocean and Antarctica. *J. of Climate*, **13 (22)**, 3940–3952, doi:10.1175/1520-0442(2000)013⟨3940:ASPTIT⟩2.0.CO;2.

Holton, J. R., and G. J. Hakim, 2012: *An introduction to dynamic meteorology*. 5th ed. Academic press, 535 pp.

Hu, Y., and Q. Fu, 2007: Observed poleward expansion of the Hadley circulation since 1979. *Atmos. Chem. Phys.*, **7 (19)**, 5229–5236, doi:10.5194/acp-7-5229-2007.

Huang, H.-P., P. D. Sardeshmukh, and K. M. Weickmann, 1999: The balance of global angular momentum in a long-term atmospheric data set. *J. Geophys. Res. Atmos.*, **104 (D2)**, 2031–2040, doi:10.1029/1998JD200068.

Huang, H.-P., K. M. Weickmann, and C. J. Hsu, 2001: Trend in atmospheric angular momentum in a transient climate change simulation with greenhouse gas and aerosol forcing. *J. climate*, **14 (7)**, 1525–1534, doi:10.1175/1520-0442(2001)014⟨1525:TIAAMI⟩2.0.CO;2.

Huang, H.-P., K. M. Weickmann, and R. D. Rosen, 2003: Unusual behavior in atmospheric angular momentum during the 1965 and 1972 El Niños. *J. climate*, **16 (15)**, 2526–2539, doi:10.1175/1520-0442(2003)016⟨2526:UBIAAM⟩2.0.CO;2.

IPCC, 2013: *Climate Change 2013: The Physical Science Basis. Contribution of Working Group I to the Fifth Assessment Report of the Intergovernmental Panel on Climate Change*. Cambridge University Press, Cambridge, United Kingdom and New York, NY, USA, 1535 pp., doi:10.1017/CBO9781107415324.

Iskenderian, H., and D. A. Salstein, 1998: Regional sources of mountain torque variability and high-frequency fluctuations in atmospheric angular momentum. *Mon. Wea. Rev.*, **126 (6)**, 1681–1694, doi:10.1175/1520-0493(1998)126⟨1681:RSOMTV⟩2.0.CO;2.

Johnson, S., 2011: Notes on fft-based differentation. MIT Applied Mathematics, Massachusetts Institute of Technology.

Koteswaram, P., 1958: The easterly jet stream in the tropics. *Tellus*, **10 (1)**, 43–57, doi:10.1111/j.2153-3490.1958.tb01984.x.

Lee, S., 1999: Why are the climatological zonal winds easterly in the equatorial upper troposphere? *J. Atmos. Sci.*, **56 (10)**, 1353–1363, doi:10.1175/1520-0469(1999)056⟨1353:WATCZW⟩2.0.CO;2.

Lorenz, D. J., and E. T. DeWeaver, 2007: Tropopause height and zonal wind response to global warming in the IPCC scenario integrations. *J. Geophys. Res. Atmos.*, **112 (D10)**, doi:10.1029/2006JD008087.

Lott, F., and M. J. Miller, 1997: A new subgrid-scale orographic drag parametrization: Its formulation and testing. *Quart. J. R. Meteor. Soc.*, **123 (537)**, 101–127, doi:10.1002/qj.49712353704.

Lu, J., G. A. Vecchi, and T. Reichler, 2007: Expansion of the Hadley cell under global warming. *Geophys. Res. Lett.*, **34 (6)**, L06 805, doi:10.1029/2006GL028443.

Madden, R. A., and P. Speth, 1995: Estimates of atmospheric angular momentum, friction, and mountain torques during 1987–1988. *J. Atmos. Sci.*, **52 (21)**, 3681–3694, doi:10.1175/1520-0469(1995)052⟨3681:EOAAMF⟩2.0.CO;2.

Paek, H., and H.-P. Huang, 2012: A comparison of decadal-to-interdecadal variability and trend in reanalysis datasets using atmospheric angular momentum. *J. Climate*, **25 (13)**, 4750–4758, doi:10.1175/JCLI-D-11-00358.1.

Paek, H., and H.-P. Huang, 2013: Centennial trend and decadal-to-interdecadal variability of atmospheric angular momentum in CMIP3 and CMIP5 simulations. *J. Climate*, **26 (11)**, 3846–3864, doi:10.1175/JCLI-D-12-00515.1.

Peixoto, J., and A. Oort, 1992: *Physics of Climate*. American Institute of Physics, 520 pp.

Poli, P., and Coauthors, 2013: The data assimilation system and initial performance evaluation of the ECMWF pilot reanalysis of the 20th-century assimilating surface observations only (ERA-20C). ECMWF ERA Report series no. 14, 59 pp.

Poli, P., and Coauthors, 2016: ERA-20C: An atmospheric reanalysis of the twentieth century. *J. Climate*, **29 (11)**, 4083–4097, doi:10.1175/JCLI-D-15-0556.1.

Räisänen, J., 2003: CO2-induced changes in atmospheric angular momentum in CMIP2 experiments. *J. Climate*, **16 (1)**, 132–143, doi:10.1175/1520-0442(2003)016⟨0132:CICIAA⟩2.0.CO;2.

Ramaswamy, V., and Coauthors, 2001: Stratospheric temperature trends: Observations and model simulations. *Rev. Geophys.*, **39 (1)**, 71–122, doi:10.1029/1999RG000065.

Reichler, T., M. Dameris, and R. Sausen, 2003: Determining the tropopause height from gridded data. *Geophys. Res. Lett.*, **30 (20)**, 2042, doi:10.1029/2003GL018240.

Rosen, R. D., and D. A. Salstein, 1983: Variations in atmospheric angular momentum on global and regional scales and the length of day. *J. Geophys. Res. Oceans*, **88 (C9)**, 5451–5470, doi:10.1029/JC088iC09p05451.

Rosen, R. D., D. A. Salstein, T. M. Eubanks, J. O. Dickey, and J. A. Steppe, 1984: An El Niño signal in atmospheric angular momentum and earth rotation. *Science*, **225 (4660)**, 411–414, doi:10.1126/science.225.4660.411.

Schneider, T., 2006: The general circulation of the atmosphere. *Annu. Rev. Earth Planet. Sci.*, **34 (1)**, 655–688, doi:10.1146/annurev.earth.34.031405.125144.

Seidel, D. J., and W. J. Randel, 2006: Variability and trends in the global tropopause estimated from radiosonde data. *J. Geophys. Res. Atmos.*, **111 (D21)**, D21 101, doi:10.1029/2006JD007363.

Simmons, A. J., and D. M. Burridge, 1981: An energy and angular-momentum conserving vertical finite-difference scheme and hybrid vertical coordinates. *Mon. Wea. Rev.*, **109 (4)**, 758–766, doi:10.1175/1520-0493(1981)109⟨0758:AEAAMC⟩2.0.CO;2.

Trenberth, K. E., 1991: Climate diagnostics from global analyses: Conservation of mass in ECMWF analyses. *J. Climate*, **4 (7)**, 707–722, doi:10.1175/1520-0442(1991)004⟨0707:CDFGAC⟩2.0.CO;2.

Trenberth, K. E., 1995: Truncation and use of model-coordinate data. *Tellus A*, **47 (3)**, 287–303, doi:10.1034/j.1600-0870.1995.t01-1-00001.x.

Trenberth, K. E., and L. Smith, 2005: The mass of the atmosphere: A constraint on global analyses. *Journal of Climate*, **18 (6)**, 864–875, doi:10.1175/JCLI-3299.1.

Weickmann, K. M., G. N. Kiladis, and P. D. Sardeshmukh, 1997: The dynamics of intraseasonal atmospheric angular momentum oscillations. *J. Atmos. Sci.*, **54 (11)**, 1445–1461, doi:10.1175/1520-0469(1997)054⟨1445:TDOIAA⟩2.0.CO;2.

WMO, 1957: Definition of the tropopause. *WMO Bull*, **6**, 136.

Yin, J. H., 2005: A consistent poleward shift of the storm tracks in simulations of 21st century climate. *Geophy. Res. Lett.*, **32 (18)**, L18 701, doi:10.1029/2005GL023684.